Scaling laws in supply limited Aeolian sand transport

Sandesh Kamath[1], Yaping Shao[1], Eric J. R. Parteli[2]

[1]Institute of Geophysics and Meteorology, University of Cologne, Germany
[2]Faculty of Physics, University of Duisburg-Essen, Germany

Key Points:

- We introduce a particle-based model in investigating Aeolian (wind-blown) sand transport when the sand cover on the soil is sparse
- The scaling of the Aeolian transport rate with the wind shear velocity has a dependency on the sand cover thickness
- There is an anomaly in the functional dependence of the transport rate on the sand cover thickness, depending on the rigid ground roughness

Corresponding author: Sandesh Kamath, skamath@uni-koeln.de

Abstract

Previous studies of wind-blown sand have considered either fully erodible or non-erodible soils, but the transport over sparsely sand-covered soils is still poorly understood. The quantitative modeling of this transport is important for the parametrization of Aeolian processes under limited sediment supply in climate models. Here we show, by means of particle-based numerical simulations, that the Aeolian sand transport rate Q scales with the wind shear velocity u_* as $Q \propto [1 + b \cdot (u_*/u_{*\mathrm{t}} - 1)] \cdot \rho_\mathrm{f} \cdot \left(u_*^2 - u_{*\mathrm{t}}^2\right)$, where $u_{*\mathrm{t}}$ is the minimal threshold u_* for sustained transport, ρ_f is air density, and b is an empirical parameter which scales, approximately, with the inverse of the mobile sand cover thickness. Therefore, the scaling of Q with u_* increases from quadratic to cubic as soil conditions change from fully erodible to rigid. Furthermore, this scaling is affected by the roughness of the non-erodible ground, thus providing constraints for modeling supply limited soils.

Plain Language Summary

The transport of sand by wind shapes the Earth's surface and constitutes one major factor for the emission of dust aerosols. The accurate modeling of wind-blown sand transport is thus important to achieve reliable climate simulations and to make predictions about the propagation of desertification. Previous models of wind-blown sand were designed to compute sand transport rates over a thick sand layer, such as the surface of large, active sand dunes. However, natural soils encompass a broad range of limited sand supply conditions, such as crusted or bare soils. It has been a long-standing open question how wind-blown sand transport rates respond to wind velocity when the bare ground is covered by a thin layer of sand. Here we calculate the trajectories of wind-blown sand grains and find that sand transport rates increase faster with wind speed under supply limited conditions than over sand dunes. The reason for this behavior is elucidated in our simulations: The hopping sand grains fly higher the less sand is covering the hard surface. We obtain mathematical expressions for the sand transport rates as a function of the thickness of sand covering the bare soil, which will be important to improve climate models.

1 Introduction

Aeolian (wind-blown) sand transport produces ripples and dunes and plays a vital role in shaping the Earth's surface. This transport occurs mainly through sand grains hopping along the surface (saltation), thereby transferring to the ground momentum that may set new particles into hopping, rolling or sliding motion (Bagnold, 1941; Shao, 2008; Kok et al., 2012). Furthermore, the particle splash generated by saltating grains provides one main mechanism of dust aerosol emission (Gillette, 1981; Shao et al., 1993), which has major feedbacks with the biosphere, the hydrological cycle and various other components of the Earth system (Mahowald et al., 2014; Schepanski, 2018). The accurate modeling of wind-blown sand is, thus, important for the development of reliable geomorphodynamic, climate and Earth system models (Shao, 2008).

Indeed, previous models of Aeolian sediment transport focused mainly on the transport over either fully erodible beds, such as migrating dunes and ripples (Anderson & Haff, 1988; Shao & Li, 1999; Sauermann et al., 2001; Almeida et al., 2008; Kok & Renno, 2009; Lämmel et al., 2012; Pähtz et al., 2014; Comola et al., 2019), or rigid, fully non-erodible beds, such as consolidated dunes and bare soils (Ho et al., 2011). These studies have shown that wind-blown transport rates follow either a quadratic or a cubic scaling with the wind shear velocity u_* — which is proportional to the mean flow velocity gradient in turbulent boundary layer flow — depending upon the bed being fully erodible or fully non-erodible, respectively (Creyssels et al., 2009; Ho et al., 2011). Moreover, a quartic scaling of the sand flux with u_*, characterizing a collisional or intense transport regime where the saltation layer is connected to the granular bed through an intermediate granular layer of intense mid-air

collisions, has been reported for fully erodible bed conditions when u_* exceeds about $4u_{*\mathrm{t}}$, where $u_{*\mathrm{t}}$ stands for the minimal threshold for sustained sand transport (Pähtz & Durán, 2020; Ralaiarisoa et al., 2020). However, natural Aeolian systems encompass a broad range of soil types subjected to limited sediment supply conditions, including bare and crusted soils sparsely covered with mobile sediments (Shao, 2008; Amir et al., 2014). The characteristics of Aeolian sand transport over such types of soil, i.e., when the thickness of the mobile sand layer on the rigid ground is comparable to a few grain diameters, are poorly understood.

The quantitative understanding of these characteristics is important for various fields, in particular to improving wind-blown sand and dust schemes in climate models. Once in the atmospheric circulation, dust substantially affects the planet's climate and biosphere, atmospheric geochemistry, the hydrological cycle, and various other components of the Earth system, yet estimates of vertical dust flux and atmospheric dust budget are counted amongst the largest uncertainty sources in climate simulations (Shao, 2008; Kok et al., 2012; Mahowald et al., 2014; Schepanski, 2018). Since dust is rarely entrained directly by wind but is, instead, emitted mainly by the impacts of wind-blown sand grains onto the ground (Shao et al., 1993), an accurate model for the Aeolian sand transport rates over various types of soil, from fully erodible to fully non-erodible, is required. However, it is difficult to derive such a model from analytical computations alone, given the broad range of natural soil erodibility conditions associated with sparsely covered bare, gravel and crusted soils (Shao, 2008; Amir et al., 2014; Macpherson et al., 2008; Wang et al., 2011).

Therefore, here we perform the direct computation of grain trajectories during Aeolian sand transport by means of particle-based simulations, or Discrete-Element-Method (DEM). This type of simulation has been applied previously to investigate Aeolian transport over fully erodible beds (Carneiro et al., 2011; Durán et al., 2012; Comola et al., 2019), thereby introducing a helpful means to elucidate processes that are difficult to assess in wind tunnel or field experiments, such as the mechanisms of sediment transport very close to the bed. Indeed, using DEM simulations, it is possible to resolve these mechanisms, as well as their impact on the resulting sand flux, without any need for assumptions about the splash process, the rebound dynamics or the modification of the wind profile in the transport layer – which are rather directly computed. As we discuss in the subsequent sections, our DEM simulations show that the scaling of the sand flux with u_* displays considerable and yet unreported dependence on the sediment supply, which is characterized in our model through the thickness of the mobile sediment layer covering the non-erodible surface underneath.

2 Numerical experiments

The Discrete-Element-Method consists of solving the Newton's equations of motion for all particles in the system under consideration of the main forces acting on them (Cundall & Strack, 1979). In contrast to other types of numerical models of soil erosion (Anderson & Haff, 1988; Almeida et al., 2008; Kok & Renno, 2009), DEM models of Aeolian sand transport do not rely, thus, on a splash function to represent the ejection of particles from the soil owing to grain-bed collisions. Rather, the lift-off velocities of the rebound and ejected particles are obtained by directly solving their equations of motion under consideration of particle-particle interactions (Lämmel et al., 2017; Yin et al., 2021).

In this section we explain the main features of our simulations, while the details about the DEM method and the integration of the equations of motion are reviewed in the Supplemental Material. We start our simulations by pouring sand-sized spherical particles of diameter d uniformly distributed in the range $160 \leq d/\mu\mathrm{m} \leq 240$ onto a flat horizontal rigid bed at the bottom of the simulation domain — which has dimensions $(L_x \times L_y \times L_z)/d_\mathrm{m} = (200 \times 8 \times 1000)$, with $d_\mathrm{m} = 200\,\mu\mathrm{m}$ denoting the mean grain size (Fig. 1). In doing so, we generate a thin bed of N_p randomly poured particles on the ground, where the bed thickness $h_{\mathrm{mob},0}$ is determined by N_p. For instance, $N_\mathrm{p} = 30,000$ for the largest bed thickness investigated here, i.e., $h_{\mathrm{mob},0} \approx 15\,d_\mathrm{m}$.

Furthermore, we adopt periodic boundary conditions in the along-wind (x) and cross-wind (y) directions and impose a reflective horizontal wall at the top of the simulation domain, to avoid that particles escape through crossing the upper boundary at $z = L_z$. However, we find that removing this reflective wall would allow only few particles for escaping, thus leading to a negligible change in the results of our simulations.

Once the particles come to rest and the bed has been formed, a few particles are injected into the simulation domain to impact on the ground; thus producing a splash and ejecting grains into air. The Aeolian drag force on the particles is computed with the expression,

$$\mathbf{F}_i^{\mathrm{d}} = -\frac{\pi d^2}{8}\rho_{\mathrm{f}} C_{\mathrm{d}} \upsilon_{\mathrm{r}} \mathbf{v}_{\mathrm{r}}, \tag{1}$$

where $\rho_{\mathrm{f}} = 1.225\,\mathrm{kg/m^3}$ is the air density, $\mathbf{v}_{\mathrm{r}} = \mathbf{v}_{\mathrm{p}} - \mathbf{u}$, with $\mathbf{v}_{\mathrm{p}}$ and $\mathbf{u}$ denoting the velocities of the particle and the fluid, respectively. Furthermore, $\upsilon_{\mathrm{r}} = |\mathbf{v}_{\mathrm{r}}|$, and C_{d} is the drag coefficient, which is computed using the following model (Cheng, 1997),

$$C_{\mathrm{d}} = \left[\left(\frac{32}{\mathrm{Re}}\right)^{2/3} + 1\right]^{3/2}, \tag{2}$$

where the Reynolds number $\mathrm{Re} = \rho_{\mathrm{f}} \upsilon_{\mathrm{r}} d_{\mathrm{m}}/\mu$, with $\mu = 1.8702 \times 10^{-5}\,\mathrm{kg\,m^{-1}s^{-1}}$ denoting the dynamic viscosity of the air. The wind velocity profile is constant along x and y throughout the simulations, while the initial vertical profile of the horizontal (downstream) wind velocity, $u_x(z)$, is logarithmic, i.e.,

$$u_x(z) = \frac{u_*}{\kappa} \ln \frac{z - h_0 + z_0}{z_0} \tag{3}$$

where u_* is the wind shear velocity, $\kappa = 0.4$ the von Kármán constant, $z_0 \approx d_{\mathrm{m}}/30$ is the roughness of the quiescent bed, and h_0 is the bed height, which is set as the uppermost height within the granular surface where the particles move with velocity smaller than $0.1\,u_*$ (Carneiro et al., 2011). However, the acceleration of the particles owing to the action of the drag force extracts momentum from the air (Owen, 1964; Anderson & Haff, 1988), thus leading to a modification of the wind velocity profile. The modified velocity profile is obtained by numerical integration of (Carneiro et al., 2011)

$$\frac{\partial u_x}{\partial z} = \frac{u_{\tau,x}(z)}{\kappa z};\; u_{\tau,x}(z) = u_* \left[1 - \frac{\tau_{\mathrm{p}}(z)}{\rho_{\mathrm{f}} u_*^2}\right]^{1/2}, \tag{4}$$

where $\tau_{\mathrm{p}}(z)$ is the grain-borne shear stress and is given by

$$\tau_{\mathrm{p}}(z) \approx \sum_{i:z_j>z} \frac{F_{i,x}^{\mathrm{d}}}{A}, \tag{5}$$

with $F_{i,x}^{\mathrm{d}}$ denoting the horizontal component of the drag force on particle i and $A = L_x \cdot L_y$ represents the cross section area parallel to the ground.

Furthermore, in order to obtain a rough rigid bed underneath the mobile sand cover, we deposit the mobile particles on top of a sheet of "frozen" immobile particles as displayed in Fig. 1 (see Suppl. Mat. for the set of DEM particle-particle contact force equations, including the presence of the frozen particles). In doing so, the rigid bed provides a model for a fully consolidated dune surface or bare granular surface, where the constituent immobile particles have the same diameter as the mobile grain size.

3 Results and discussion

Once transport begins, some of the grains composing the initial bed layer are entrained into flow, so that the bed layer thickness — which has initial value $h_{\mathrm{mob},0}$ at time $t = 0$ —

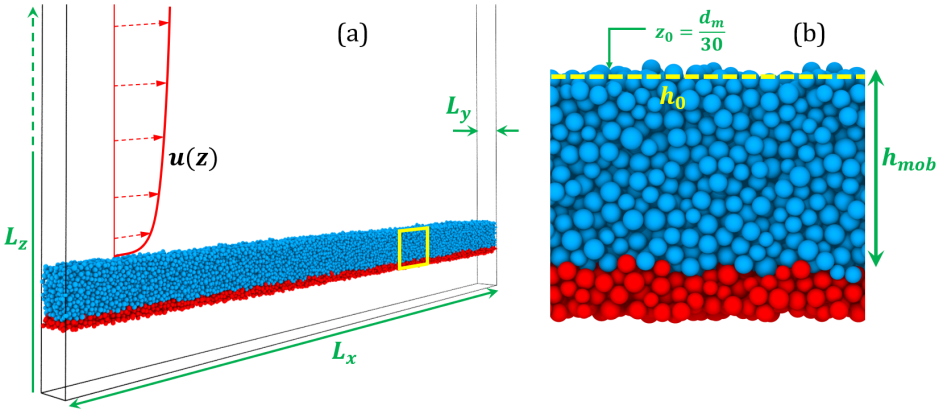

Figure 1: (a) Snapshot of the numerical experiment at $t = 0$, indicating the dimensions of the simulation domain and the undisturbed wind profile. (b) Side-view of an excerpt of the sediment bed, displaying a layer of mobile particles (blue) of thickness $h_{\mathrm{mob},0}$ on top of the immobile particles constituting the rough ground.

decreases over time until transport eventually achieves steady state. At steady state, the bed layer thickness adopts then a slightly smaller value, denoted here $h_{\mathrm{mob,s}}$. The dependence of $h_{\mathrm{mob,s}}$ on $h_{\mathrm{mob},0}$ is elucidated in Section 5 of the Supplemental Material.

We note that, in the type of numerical simulations considered in the present work, periodic boundary conditions are applied (see Section 2), so that the number of particles in the system is constant over time (Carneiro et al., 2011; Durán et al., 2012; Pähtz & Durán, 2020). Indeed, the domain of our simulations may be interpreted as a small stretch of soil over which the sediment flux is in the steady state. Due to fluctuations associated with the transport dynamics, the difference between the particle mass outflux from and influx into this soil stretch varies over time, but on average, the total number of particles within the associated volume is constant over time. Here we use the initial mobile layer thickness $h_{\mathrm{mob},0}$ to characterize the sediment supply in the model and focus on the role of this sediment supply for the scaling of the sediment flux with u_*. However, using the equations provided in Section 5 of the Supplemental Material, and in view of the considerations above, the results discussed next may be expressed in terms of $h_{\mathrm{mob,s}}$ too.

We begin our discussion by considering the largest initial mobile sediment layer thickness, $h_{\mathrm{mob},0} = 15\,d_{\mathrm{m}}$. We find that, by starting with this value of $h_{\mathrm{mob},0}$, transport conditions at steady state ($h_{\mathrm{mob,s}} \approx 14\,d_{\mathrm{m}}$; see Suppl. Mat.) correspond to the fully erodible bed scenario reported in previous studies. Specifically, our simulations reproduce quantitatively the value of the height-integrated, non-suspended mass flux of transported particles, Q, as a function of u_*, and the observation that, for moderate wind conditions ($u_*/u_{*\mathrm{t}} \lesssim 4$), Q is approximately proportional to $\tau - \tau_{\mathrm{t}}$, with $\tau = \rho_{\mathrm{f}} u_*^2$ denoting the mean shear stress of the turbulent wind flow over the surface, and $\tau_{\mathrm{t}} = \rho_{\mathrm{f}} u_{*\mathrm{t}}^2$ corresponding to the minimal threshold value of τ for sand transport (Fig. 2). Furthermore, our numerical predictions match the experimental observations of the nearly exponential decay of the vertical particle concentration profile above the ground and the minimal threshold wind shear velocity $u_{*\mathrm{t}} \approx 0.165\,\mathrm{m/s}$ predicted for the mean particle size in our simulations (see Suppl. Mat., Fig. S1).

However, as we decrease the initial bed layer thickness $h_{\mathrm{mob},0}$ substantially, we observe a change in the scaling of the steady-state sediment flux with u_*. More precisely, our

simulation results follow, approximately, the expression,

$$Q = \left\{ a \cdot \left[1 + b \cdot \left(\frac{u_*}{u_{*\mathrm{t}}} - 1 \right) \right] \right\} \cdot [\tau - \tau_\mathrm{t}], \tag{6}$$

where $a \approx 0.1\,\mathrm{s}$, and b can be approximately described as

$$b \approx k_0 \left(\frac{h_{\mathrm{mob},0}}{d_\mathrm{m}} - c_0 \right)^{-1} \tag{7}$$

with $k_0 \approx 0.25$ and $c_0 \approx 0.15$ denoting empirical parameters.

Wind tunnel experiments (Ho et al., 2011) revealed a cubic scaling of Q with u_* on fully rigid beds. Here, we find that sediment transport rates over a soil that is not fully rigid but contains, instead, a thin layer of mobile sediment, further depends on this layer's thickness according to Eqs. (6) and (7). Specifically, our simulations reveal a fast decrease of the coefficient b in Eq. (7) with the bed layer thickness, such that transport conditions consistent with fully erodible bed scenarios are observed from values of this thickness comparable to the particle diameter. More precisely, as shown in Fig. 2, the quadratic scaling of Q with u_* characteristic of transport over dense sand beds is recovered already at very low values of the bed layer thickness in the range between $1 - 2\,d_\mathrm{m}$.

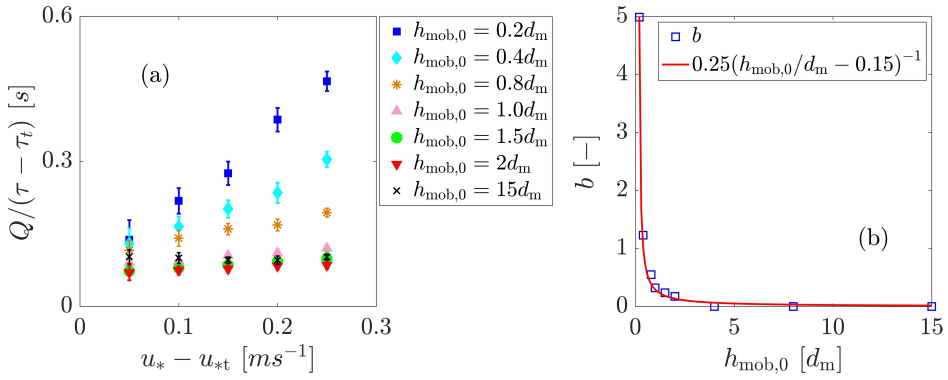

Figure 2: (a) Sand flux Q rescaled with the excess shear stress, $\tau - \tau_\mathrm{t}$, plotted as a function of $(u_* - u_{*\mathrm{t}})$ for different values of $h_{\mathrm{mob},0}$. (b) The symbols denote the parameter b in Eq. (6), as obtained from the best fit to the data in (a), while the continuous line denotes the best fit using Eq. (7). Error bars denote the standard deviation from averaging over 5 s within the steady state.

To shed light on the microscopic origin of Eq. (6), we note that momentum conservation yields $Q = [\ell_\mathrm{hop}/(u_{0\downarrow} - u_{0\uparrow})] \cdot [\tau - \tau_\mathrm{t}]$ (Bagnold, 1941; Sørensen, 2004; Ho et al., 2011), where ℓ_hop denotes the mean hop length of the saltating particles, while $u_{0\downarrow}$ and $u_{0\uparrow}$ are their mean horizontal impact and lift-off velocities, respectively. Furthermore, ℓ_hop and $u_{0\downarrow} - u_{0\uparrow}$ (computed as explained in Section 4 of the Suppl. Mat.) are related to the mean horizontal grain velocity $u_0 = (u_{0\downarrow} + u_{0\uparrow})/2$ (or slip velocity) through the approximate scaling expressions $\ell_\mathrm{hop} \propto u_0^2/g$ and $u_{0\downarrow} - u_{0\uparrow} \propto u_0$ (Ho et al., 2011), which leads to

$$Q \approx C_u \cdot \frac{u_0}{g} \cdot [\tau - \tau_\mathrm{t}] \tag{8}$$

where C_u is an empirical parameter. An increase in u_* over a fully erodible bed leads to an enhancement of the particle concentration in the transport layer, without significantly affecting u_0 (Ho et al., 2011). This independence between u_0 and u_* underlies the quadratic

scaling of the sand flux Q with u_* by virtue of Eq. (8). By contrast, the transport layer over the hard surface is, for a given saltation flux, much thicker than over an erodible bed because of the non-saturated feedback which keeps a larger wind velocity in the saltation layer (Ho et al., 2011). The weak coupling between the particles and the wind in the transport layer over a fully non-erodible surface results in a linear scaling of u_0 with u_*, thus yielding a cubic scaling of Q with u_* in view of Eq. (8) (Ho et al., 2011).

Here we find that, in the presence of a thin layer of mobile sand on the hard ground, the scaling of the grain slip velocity u_0 with the wind shear velocity u_* further depends on the mobile sand layer thickness, as elucidated through Fig. 3c. We find that

$$C_u \cdot \frac{u_0}{g} \approx a \cdot \left[1 + b \cdot \left(\frac{u_*}{u_{*\mathrm{t}}} - 1\right)\right] \tag{9}$$

with $C_u \approx 1.8$, where the RHS of Eq. (9) is equal to the term inside the curly braces in Eq. (6), i.e., including the values of the parameters a and b estimated from Fig. 2. Therefore, Eqs. (8) and (9) elucidate the microscopic origin of the supply-dependent scaling of the sand flux with u_* obtained in our simulations, i.e., Eq. (6). We find that the grain slip velocity is nearly independent of u_* when steady-state transport conditions correspond to a bed layer thickness larger than about $1 - 2\,d_\mathrm{m}$.

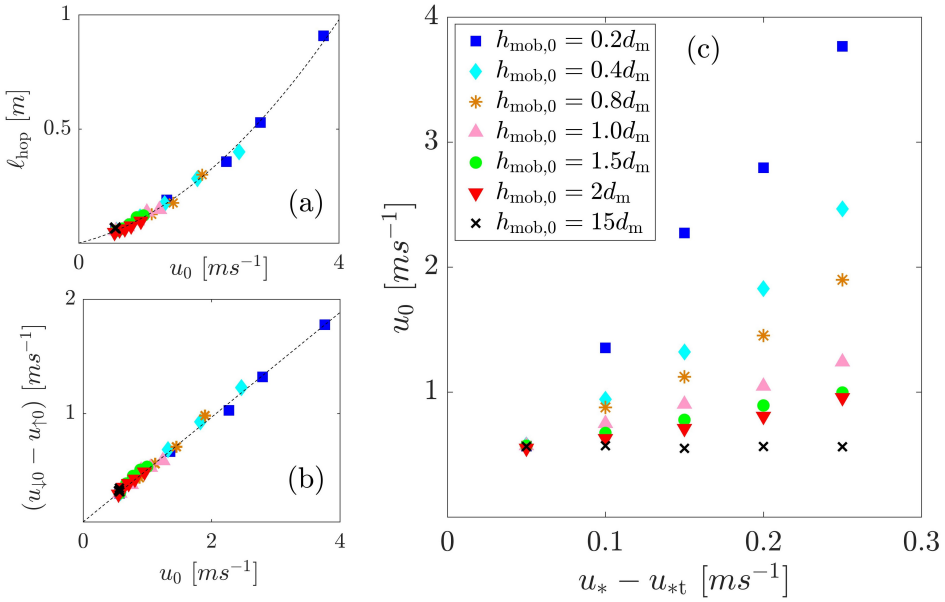

Figure 3: (a) Mean hop length, ℓ_{hop}, and (b) difference between the mean grain horizontal velocities at impact and lift-off, $u_{0\downarrow} - u_{0\uparrow}$, as a function of the slip velocity u_0. The dashed lines in (a) and (b) denote the expressions $\ell_{\mathrm{hop}} \approx 0.065u_0^2$ and $u_{0\downarrow} - u_{0\uparrow} \approx 0.43u_0$, respectively, obtained from the best fits to the simulation data. In (c), the slip velocity is shown as a function of $u_* - u_{*\mathrm{t}}$ for different values of $h_{\mathrm{mob},0}$. The legend in (c) applies as well to both (a) and (b).

To the best of our knowledge, our study is the first one to estimate sediment transport rates from direct numerical simulations of particle trajectories under intermediate soil erodibility conditions between fully erodible and fully non-erodible. We find that our results remain approximately valid when the rigid bed underneath the mobile sediment layer is a smooth flat surface. However, the immobile roughness elements on the hard ground have a crucial effect on the value of the Aeolian sand flux, which we discuss next.

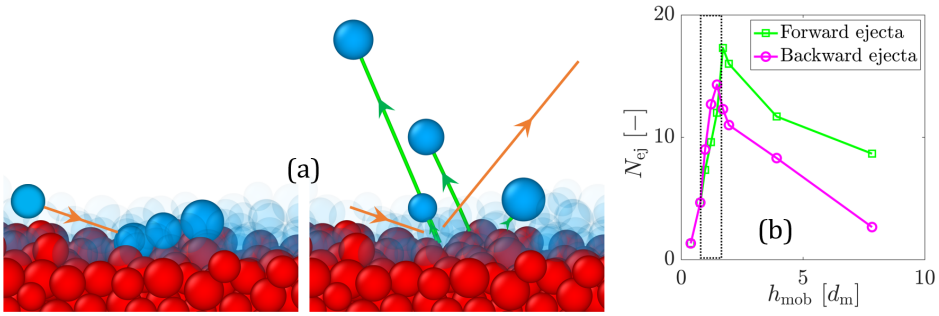

Figure 4: By means of granular splash numerical experiments with impact angles and velocities characteristic of wind-blown sand transport (a), we find that most ejected grains have negative horizontal lift-off velocity, when the value of the bed layer thickness is $\lesssim 2\,d_m$, and positive otherwise (b). The snapshots correspond to a simulation using a bed layer thickness $\approx 2\,d_m$. Most of the mobile (blue) particles lying on the rigid grains (red) have been rendered transparent for better visualization of the splashed particles.

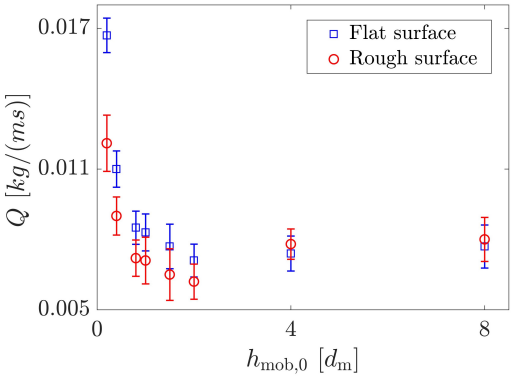

Figure 5: Sand flux Q as a function of $h_{mob,0}$, obtained with $u_* = 0.30\,\mathrm{m/s}$. We considered the non-erodible surface consisting of a smooth flat ground (blue) and immobile particles (red).

In the regime where saltating particles collide onto a sand bed of thickness $\lesssim 2\,d_m$, and in the presence of roughness elements on the hard ground underneath, sand particles are ejected through splash events mainly *backwards*, i.e., the majority of ejecta displays negative horizontal lift-off velocity component. This result can be understood by noting that, as downwind hopping grains impact obliquely upon the thin sand layer covering the rough ground, they mobilize soil grains forward, which, however, collide with the roughness elements located in their front. Upon such collisions, the trajectories of the bed particles mobilized by grain-bed impacts are reflected backwards, as elucidated through our granular splash experiments (Fig. 4, where N_{ej} is the number of ejected grains per impact), thus yielding a negative mean horizontal lift-off velocity. These dynamics lead to an anomaly in the dependence of the steady-state sand flux Q on the bed layer thickness, with the emergence of a minimum flux value around $h_{mob,0} \approx 2\,d_m$ (or $h_{mob,s} \approx 1.8\,d_m$), which is not observed when the ground is a smooth flat surface (Fig. 5). Furthermore the value of the bed layer thickness associated with the minimum flux is independent of u_*, thus indicating that the anomaly reported here is purely a signature of the soil erodibility conditions and is not affected by the flow properties.

We note that, notwithstanding the strong decrease of N_{ej} with the bed layer thickness in the fully erodible bed regime (as can be seen in Fig. 4b), the steady-state sand flux Q is only weakly affected by the amount of mobile grains on the ground when this thickness is larger than about $1 - 2\,d_{\mathrm{m}}$, as can be seen from Fig. 1. Therefore, our simulation results are providing evidence in support of the hypothesis that the magnitude of Q is controlled by the rebound dynamics of sand grains during transport — as assumed, for instance, in a recent purely rebound-based model (Pähtz et al., 2021) — rather than by the splash process. Our results further help to elucidate the observation that cohesion, which affects mainly the splash process by enhancing particle-particle attractive interaction forces within the bed, has little impact on the steady-state sediment mass flux and the threshold for Aeolian transport cessation, as these are mainly controlled by rebound dynamics (Comola et al., 2019).

Our model reproduces the different scaling laws of the Aeolian sand flux with the wind shear velocity observed experimentally, both over fully erodible and rigid beds (Figs. 2 and S1). However, various ingredients that are essential to improve the quantitative assessment of Aeolian sand flux, such as complex particle geometric shapes and aerodynamic entrainment (Li et al., 2020), should be incorporated in future work. Furthermore, we have employed sand-sized non-erodible roughness elements, but natural soils encompass much broader particle size distributions, including the presence of gravels, pebbles and rocks on the ground. Based on the results of our simulations, we expect that such coarser non-erodible elements have even larger impacts on the scaling laws of Aeolian sand transport rates.

Previous work developed continuum models for Aeolian flux that explicitly account for the effect of low sediment supply and spatio-temporal variations in bed surface properties, including moisture, shells, non-erodible elements and vegetation (De Vries et al., 2014; Hoonhout & Vries, 2016). Furthermore, the particle-based simulations adopted in the present work provide a means to improve our understanding of the (microscopic) particle-scale mechanisms controlling the response of Aeolian transport processes to different types of soil and particle-bed interactions. Future research combining insights from both types of model could thus help to achieve improved numerical simulations of Aeolian soil morphodynamic processes at different scales (Werner, 1995; Kroy et al., 2002; Durán et al., 2010), by incorporating the effect of sediment supply on sediment flux and erosion/deposition rates.

4 Conclusions

In conclusion, we have presented the first numerical model for wind-blown sand flux under supply limited conditions, by characterizing this flux as a function of the thickness of the mobile sediment layer available for transport on the ground. Specifically, we showed that the Aeolian sand flux scales with the excess shear stress multiplied by a coefficient that decreases with the mobile layer thickness covering the non-erodible ground, thereby yielding a model for Aeolian transport rates under intermediate bed erodibility conditions between the fully erodible and fully non-erodible scenarios. Our model elucidates how the scaling of the Aeolian sand flux Q with the wind shear velocity u_* changes from quadratic to cubic as bed conditions change from fully erodible to fully non-erodible, respectively (Ho et al., 2011).

We also found that the roughness elements on the rigid bed affect the sediment flux under low supply conditions by causing an anomaly in the behavior of Q with the bed layer thickness, with the occurrence of a minimum which is independent on the flow conditions. These findings will have an implication for the representation of non-erodible elements associated with different types of soil in future experimental and theoretical studies.

Acknowledgments

All data included in this work are generated from our numerical model and is available online (https://doi.org/10.6084/m9.figshare.17942519). The data for validation with experiments

is available from (Creyssels et al., 2009). We thank the German Research Foundation (DFG) for funding through the Heisenberg Programme and the grant - 348617785.

References

Almeida, M. P., Parteli, E. J. R., Andrade, J. S., & Herrmann, H. J. (2008). Giant saltation on mars. *Proceedings of the National Academy of Sciences*, *105*(17), 6222–6226. doi: https://doi.org/10.1073/pnas.0800202105

Amir, R., Kinast, S., Tsoar, H., Yizhaq, H., Zaady, E., & Ashkenazy, Y. (2014). The effect of wind and precipitation on vegetation and biogenic crust covers in the sde-hallamish sand dunes. *Journal of Geophysical Research: Earth Surface*, *119*(3), 437–450. doi: https://doi.org/10.1002/2013JF002944

Anderson, R. S., & Haff, P. K. (1988). Simulation of eolian saltation. *Science*, *241*(4867), 820–823. doi: https://doi.org/10.1126/science.241.4867.820

Bagnold, R. A. (1941). *The physics of blown sand and desert dunes.* Methuen, London.

Carneiro, M. V., Pähtz, T., & Herrmann, H. J. (2011). Jump at the onset of saltation. *Physical Review Letters*, *107*(9), 098001. doi: https://doi.org/10.1103/PhysRevLett.107.098001

Cheng, N.-S. (1997). Simplified settling velocity formula for sediment particle. *Journal of hydraulic engineering*, *123*(2), 149–152.

Comola, F., Gaume, J., Kok, J., & Lehning, M. (2019). Cohesion-induced enhancement of aeolian saltation. *Geophysical Research Letters*, *46*(10), 5566–5574. doi: https://doi.org/10.1029/2019GL082195

Creyssels, M., Dupont, P., El Moctar, A. O., Valance, A., Cantat, I., Jenkins, J. T., ... Rasmussen, K. R. (2009). Saltating particles in a turbulent boundary layer: experiment and theory. *J. Fluid Mechanics*, *625*, 47. doi: https://doi.org/10.1017/S0022112008005491

Cundall, P. A., & Strack, O. D. (1979). A discrete numerical model for granular assemblies. *geotechnique*, *29*(1), 47–65. doi: https://doi.org/10.1680/geot.1979.29.1.47

De Vries, S., de Vries, J. v. T., Van Rijn, L., Arens, S., & Ranasinghe, R. (2014). Aeolian sediment transport in supply limited situations. *Aeolian Research*, *12*, 75–85. doi: https://doi.org/10.1016/j.aeolia.2013.11.005

Durán, O., Andreotti, B., & Claudin, P. (2012). Numerical simulation of turbulent sediment transport, from bed load to saltation. *Physics of Fluids*, *24*(10), 103306. doi: https://doi.org/10.1063/1.4757662

Durán, O., Parteli, E. J., & Herrmann, H. J. (2010). A continuous model for sand dunes: Review, new developments and application to barchan dunes and barchan dune fields. *Earth Surface Processes and Landforms*, *35*(13), 1591-1600. doi: https://doi.org/10.1002/esp.2070

Gillette, D. A. (1981). Production of dust that may be carried great distances. In *Desert Dust: Origin, Characteristics, and Effect on Man.* Geological Society of America. doi: https://doi.org/10.1130/SPE186-p11

Ho, T. D., Valance, A., Dupont, P., & El Moctar, A. O. (2011). Scaling laws in aeolian sand transport. *Physical Review Letters*, *106*(9), 094501. doi: https://doi.org/10.1103/PhysRevLett.106.094501

Hoonhout, B. M., & Vries, S. d. (2016). A process-based model for aeolian sediment transport and spatiotemporal varying sediment availability. *Journal of Geophysical Research: Earth Surface*, *121*(8), 1555–1575. doi: https://doi.org/10.1002/2015JF003692

Kok, J. F., Parteli, E. J., Michaels, T. I., & Karam, D. B. (2012). The physics of wind-blown sand and dust. *Reports on progress in Physics*, *75*(10), 106901. doi: https://doi.org/10.1088/0034-4885/75/10/106901

Kok, J. F., & Renno, N. O. (2009). A comprehensive numerical model of steady state saltation (comsalt). *Journal of Geophysical Research: Atmospheres*, *114*(D17). doi: https://doi.org/10.1029/2009JD011702

Kroy, K., Sauermann, G., & Herrmann, H. J. (2002, Sep). Minimal model for aeolian sand dunes. *Phys. Rev. E*, *66*, 031302. doi: https://doi.org/10.1103/PhysRevE.66.031302

Lämmel, M., Dzikowski, K., Kroy, K., Oger, L., & Valance, A. (2017). Grain-scale modeling and splash parametrization for aeolian sand transport. *Phys. Rev. E*, *95*, 022902. doi: https://doi.org/10.1103/PhysRevE.95.022902

Lämmel, M., Rings, D., & Kroy, K. (2012). A two-species continuum model for aeolian sand transport. *The New Journal of Physics*, *14*(9), 093037. doi: https://doi.org/10.1088/1367-2630/14/9/093037

Li, G., Zhang, J., Herrmann, H. J., Shao, Y., & Huang, N. (2020). Study of aerodynamic grain entrainment in aeolian transport. *Geophysical Research Letters*, *47*(11), e2019GL086574. doi: https://doi.org/10.1029/2019GL086574

Macpherson, T., Nickling, W. G., Gillies, J. A., & Etyemezian, V. (2008). Dust emissions from undisturbed and disturbed supply-limited desert surfaces. *Journal of Geophysical Research: Earth Surface*, *113*(F2). doi: https://doi.org/10.1029/2007JF000800

Mahowald, N., Albani, S., Kok, J. F., Engelstaeder, S., Scanza, R., Ward, D. S., & Flanner, M. G. (2014). The size distribution of desert dust aerosols and its impact on the earth system. *Aeolian Research*, *15*, 53-71. doi: https://doi.org/10.1016/j.aeolia.2013.09.002

Owen, P. R. (1964). Saltation of uniform grains in air. *Journal of Fluid Mechanics*, *20*(2), 225-242. doi: https://doi.org/10.1017/S0022112064001173

Pähtz, T., & Durán, O. (2020). Unification of aeolian and fluvial sediment transport rate from granular physics. *Physical review letters*, *124*(16), 168001. doi: https://doi.org/10.1103/PhysRevLett.124.168001

Pähtz, T., Liu, Y., Xia, Y., Hu, P., He, Z., & Tholen, K. (2021). Unified model of sediment transport threshold and rate across weak and intense subaqueous bedload, windblown sand, and windblown snow. *Journal of Geophysical Research: Earth Surface*, *126*(4), e2020JF005859. doi: https://doi.org/10.1029/2020JF005859

Pähtz, T., Parteli, E. J. R., Kok, J. F., & Herrmann, H. J. (2014). Analytical model for flux saturation in sediment transport. *Physical Review E*, *89*(5), 052213. doi: https://doi.org/10.1103/PhysRevE.89.052213

Ralaiarisoa, J., Besnard, J.-B., Furieri, B., Dupont, P., El Moctar, A. O., Naaim-Bouvet, F., & Valance, A. (2020). Transition from saltation to collisional regime in windblown sand. *Physical Review Letters*, *124*(19), 198501. doi: https://doi.org/10.1103/PhysRevLett.124.198501

Sauermann, G., Kroy, K., & Herrmann, H. J. (2001). Continuum saltation model for sand dunes. *Physical Review E*, *64*(3), 031305. doi: https://doi.org/10.1103/PhysRevE.64.031305

Schepanski, K. (2018). Transport of mineral dust and its impact on climate. *Geosciences*, *8*(5). doi: https://doi.org/10.3390/geosciences8050151

Shao, Y. (Ed.). (2008). *Physics and modelling of wind erosion*. Springer Netherlands. doi: https://doi.org/10.1007/978-1-4020-8895-7

Shao, Y., & Li, A. (1999). Numerical modelling of saltation in the atmospheric surface layer. *Boundary-Layer Meteorology*, *91*, 199-225. doi: https://doi.org/10.1023/A:1001816013475

Shao, Y., Raupach, M., & Findlater, P. (1993). Effect of saltation bombardment on the entrainment of dust by wind. *Journal of Geophysical Research: Atmospheres*, *98*(D7), 12719–12726. doi: https://doi.org/10.1029/93JD00396

Sørensen, M. (2004). On the rate of aeolian sand transport. *Geomorphology*, *59*(1-4), 53–62. doi: https://doi.org/10.1016/j.geomorph.2003.09.005

Wang, X., Zhang, C., Wang, H., Qian, G., Luo, W., Lu, J., & Wang, L. (2011). The significance of gobi desert surfaces for dust emissions in china: an experimental study. *Environmental Earth Sciences*, *64*(4), 1039–1050. doi: https://doi.org/10.1007/s12665-011-0922-2

Werner, B. T. (1995). Eolian dunes: computer simulations and attractor interpretation. *Geology*, *23*(12), 1107–1110. doi: https://doi.org/10.1130/0091-7613(1995)023⟨1107:

EDCSAA⟩2.3.CO;2

Yin, X., Huang, N., Jiang, C., Parteli, E. J., & Zhang, J. (2021). Splash function for the collision of sand-sized particles onto an inclined granular bed, based on discrete-element-simulations. *Powder Technology*, *378*, 348-358. doi: https://doi.org/10.1016/j.powtec.2020.10.008

References from the Supporting Information

Brilliantov, N. V., Spahn, F., Hertzsch, J.-M., & Pöschel, T. (1996). Model for collisions in granular gases. *Physical review E*, *53*(5), 5382. doi: https://doi.org/10.1103/PhysRevE.53.5382

Carneiro, M. V., Araújo, N. A. M., Pähtz, T., & Herrmann, H. J. (2013). Midair collisions enhance saltation. *Physical review letters*, *111*(5), 058001. doi: https://doi.org/10.1103/PhysRevLett.111.058001

Di Renzo, A., & Di Maio, F. P. (2004). Comparison of contact-force models for the simulation of collisions in dem-based granular flow codes. *Chemical Engineering Science*, *59*(3), 525-541. doi: https://doi.org/10.1016/j.ces.2003.09.037

Fan, F., Parteli, E. J. R., & Pöschel, T. (2017). Origin of granular capillarity revealed by particle-based simulations. *Phys. Rev. Lett.*, *118*, 218001. doi: https://doi.org/10.1103/PhysRevLett.118.218001

Kruggel-Emden, H., Simsek, E., Rickelt, S., Wirtz, S., & Scherer, V. (2007). Review and extension of normal force models for the discrete element method. *Powder Technol.*, *171*, 157-173. doi: https://doi.org/10.1016/j.powtec.2006.10.004

Luding, S. (2008). Cohesive, frictional powders: contact models for tension. *Granular matter*, *10*(4), 235. doi: https://doi.org/10.1007/s10035-008-0099-x

Machado, M., Moreira, P., Flores, P., & Lankarani, H. M. (2012). Compliant contact force models in multibody dynamics: Evolution of the hertz contact theory. *Mechanism and Machine Theory*, *53*, 99-121. doi: https://doi.org/10.1016/j.mechmachtheory.2012.02.010

Parteli, E. J. R., Schmidt, J., Blümel, C., Wirth, K.-E., Peukert, W., & Pöschel, T. (2014). Attractive particle interaction forces and packing density of fine glass powders. *Sci. Rep.*, *4*, 6227. doi: https://doi.org/10.1038/srep06227

Plimpton, S. (1995). Fast parallel algorithms for short-range molecular dynamics. *Journal of computational physics*, *117*(1), 1–19. (Website of the DEM solver LAMMPS: `https://lammps.sandia.gov/`) doi: https://doi.org/10.1006/jcph.1995.1039

Pöschel, T., & Schwager, T. (2005). *Computational granular dynamics.* Springer Berlin Heidelberg. doi: https://doi.org/10.1007/3-540-27720-X

Santos, A. P., Bolintineanu, D. S., Grest, G. S., Lechman, J. B., Plimpton, S. J., Srivastava, I., & Silbert, L. E. (2020). Granular packings with sliding, rolling, and twisting friction. *Phys. Rev. E*, *102*, 032903. doi: https://doi.org/10.1103/PhysRevE.102.032903

Schäfer, J., Dippel, S., & Wolf, D. E. (1996). Force Schemes in Simulations of Granular Materials. *J. Phys. I France*, *6*, 5-20. doi: https://doi.org/10.1051/jp1:1996129

Schmidt, J., Parteli, E. J., Uhlmann, N., Wörlein, N., Wirth, K.-E., Pöschel, T., & Peukert, W. (2020). Packings of micron-sized spherical particles: Insights from bulk density determination, x-ray microtomography and discrete element simulations. *Advanced Powder Technology*, *31*(6), 2293-2304. doi: https://doi.org/10.1016/j.apt.2020.03.018

Shao, Y., & Lu, H. (2000). A simple expression for wind erosion threshold friction velocity. *Journal of Geophysical Research: Atmospheres*, *105*(D17), 22437-22443. doi: https://doi.org/10.1029/2000JD900304

Silbert, L. E., Ertaş, D., Grest, G. S., Halsey, T. C., Levine, D., & Plimpton, S. J. (2001). Granular flow down an inclined plane: Bagnold scaling and rheology. *Physical Review E*, *64*(5), 051302. doi: https://doi.org/10.1103/PhysRevE.64.051302

Verbücheln, F., Parteli, E. J. R., & Pöschel, T. (2015). Helical inner-wall texture prevents jamming in granular pipe flows. *Soft Matter*, *11*(21), 4295–4305. doi: https://doi.org/10.1039/c5sm00760g